Electronic Supplementary Information

Colloidally Uniform Single Crystal Precursors Enable Uniform $FAPbI_3$ Films for Efficient Perovskite Submodules

Yugang Liang,[a] Yingping Fan,[a] Zhixiao Qin,[b] Lei Lu,[a] Haifei Wang,[a] Meng Ren,[a] Fang Liu,[a] Yanfeng Miao,[ac] Yuetian Chen*[ac] and Yixin Zhao*[acd]

[a] School of Environmental Science and Engineering, Frontiers Science Center for Transformative Molecules, Shanghai Jiao Tong University, Shanghai 200240, China.

[b] Shanghai Perovskite Technology Co.,Ltd, , Shanghai 201109, China.

[c] Shanghai Non-carbon Energy Conversion and Utilization Institute, Shanghai 200240, China.

[d] State Key Lab of Metal Matrix Composites, Shanghai Jiao Tong University, Shanghai 200240, China.

* Correspondence author: yixin.zhao@sjtu.edu.cn (Y. Zhao); yuetian.chen@sjtu.edu.cn (Y. Chen).

Materials and methods

Materials

Lead iodide (PbI_2, 99.999%), methylamine hydrochloride (MACl, 99.0%), and tin (IV) oxide colloid precursor (SnO_2, 15% in H_2O colloidal dispersion) were purchased from Aladdin. Lead iodide (PbI_2, 98%, 99%) and formamidinium iodide (FAI, 99.5%) were purchased from Macklin. Formamidine acetate was purchased from Bide Pharmatech. Hydroiodic acid was purchased from Adamas. n-octylamine hydrobromide (98.0%) and phenethylammonium iodide (PEAI, 99.5%) were purchased from GreatCell Solar Materials. 1,4-butyrolactone (anhydrous, 99.0%) was purchased from Sinopharm Chemical Reagent Co., Ltd. N, N-dimethylformamide (DMF, anhydrous, 99.8%), dimethyl sulfoxide (DMSO, anhydrous, 99.7%) and isopropanol (IPA, 99.8%) were purchased from J&K Scientific Ltd. Diethyl ether (anhydrous) and chloroform (anhydrous, 99.0%) were purchased from Sinopharm Chemical Reagent Co., Ltd.

Synthesis of low-purity Formamidinium iodide (FAI)

The synthesis was conducted employing formamidine acetate and hydroiodic acid. Specifically, 494.3g formamidine acetate and 607.5g hydroiodic acid were mixed directly in round-bottomed flask and stirred vigorously. After evaporating the solvent in a vacuum evaporator at 80 °C for an hour, yellow powder was obtained. The resulting powder was then dissolved in ethanol and precipitated with diethyl ether. After recrystallization, the obtained powder was collected and dried at 60 °C for 24 hours.

Single crystal growth

For $FAPbI_3$ single crystal, 0.6 mol synthesized FAI and 0.6 mol low-purity (98 %) PbI_2 were added into 500 mL 1,4-butyrolactone. The mixture was stirred at 25 °C for 1 h to obtain a homogeneous solution. The solution was then slowly heated to 120 °C at a rate of 10 °C per hour, and the black-phase single crystals (α-$FAPbI_3$) were collected. The yellow-phase single crystals (δ-$FAPbI_3$) were obtained when the temperature of solution was risen to 90 °C.

Small-area device fabrication

A compact TiO_2 layer of 20 nm was deposited by spray pyrolysis using 0.2 M Ti (IV) bis(ethylacetoacetate)-diisopropoxide 1-butanol solution on a cleaned, patterned and fluorine-doped tin oxide (FTO, 7 Ω sq^{-1}) substrate on a 450 °C heating plate and followed by 1 h annealing. The SnO_2 colloid precursor/ammonium solution (1:9 volume ratio) was spin-coating on the TiO_2 layer at 3000 rpm for 30 s followed by annealing for 30 min at 180 °C. The traditional PbI_2+FAI precursor was prepared by mixing high purity (> 99.5%) materials (1.5 mmol PbI_2 and 1.5 mmol FAI) and 0.525 mmol MACl in 1 mL solvent (DMF: DMSO with volume ratio of 9:1). The $FAPbI_3$ perovskite single crystal precursor was prepared by mixing 1.5 mmol $FAPbI_3$ single crystals and 0.525 mmol MACl in 1 mL solvent (DMF: DMSO with volume ratio of 9:1). The perovskite films were deposited by spin-coating on the FTO/TiO_2/SnO_2 substrate at 5000 rpm for 15 s. During spin-coating, 600 μL diethyl ether was dripped at the end of 10 s. All perovskite films were annealed at 150 °C for 15 min and further treated by the chloroform dispersion of n-octylamine hydrobromide at 5000 rpm. Hole transport layers were prepared by spin coating 0.1 M spiro-OMeTAD solution (doped with 0.035 M bis(trifluoromethane) sulfonimide lithium salt (Li-TFSI), 0.12 M 4-tert-butylpyridine (tBP) and dissolved in chlorobenzene) on perovskite layers at 3000 rpm for 30 s. Finally, a 100 nm Ag electrode was thermally evaporated on top. The fabrication process was operated in a dry-air box with less than 20% humidity. The active area of the device is 0.085 cm^2.

Large-area perovskite submodules

Firstly, FTO substrate with dimensions of 30 cm by 30 cm was etched by a picosecond laser scriber to form P1 lines with a width of 15 μm under a speed of 400 mm/s and a frequency of 450 kHz. The deposition procedures for the TiO_2 layer, the SnO_2 layer and spiro-OMeTAD layer were as same as that of small-area devices. Particularly, the 30 cm × 30 cm films were prepared using large-scale spin coating equipment (Leibo-AC300).

The PbI_2+FAI perovskite precursor solution was prepared by mixing 1.3 mmol PbI_2, 1.3 mmol FAI, and 0.45 mmol MACl in 1 mL solvent (DMF: DMSO with volume ratio of 4:1). The $FAPbI_3$ perovskite single crystal precursor was prepared by mixing 1.3 mmol $FAPbI_3$ single crystals and 0.45 mmol MACl in 1 mL solvent (DMF: DMSO with volume ratio of 4:1). The filtered perovskite precursor solution was spin-coating on the TiO_2/SnO_2 substrate at 2000 rpm for 10 s, followed by a vacuum-flashing process. All perovskite films were annealed at 150 °C for 15 min and further treated by the isopropanol dispersion of PEAI (3 mg/ml) at 5000 rpm for 30s.

P2 and P3 were etched before and after evaporating Au electrode, respectively. The scribing rate of P2 and P3 are 500 mm s^{-1} and 700 mm s^{-1}. The Q frequency of P2 and P3 are 518 kHz and 520 kHz. The power of P1, P2 and P3 are 1.25 W, 0.50 W and 0.35 W. The width of P2 and P3 are 36 μm and 25 μm. The distance between P1-P2 and P2-P3 are 30 μm and 46 μm. The geometrical fill factor is ~96%.

Film and device characterizations

Inductively coupled plasma optical emission spectrometer (ICP-OES) (Agilent ICP-OES 5110) was used at 1.20 KW RF Power, Plasma flow is 12 L/min. UV-vis spectra were collected on a Cary-60 UV-Vis spectrophotometer. Dynamic light scattering measurements were conducted on a nanoparticle analyzer (Beckman Coulter, Delsa Nano C). The XRD patterns of perovskite films were collected by Shimadzu XRD-6100 diffractometer with Cu Kα radiation. Grazing incidence wide-angle X-ray scattering (GIWAXS) measurements were performed at the BL14B1 beamline of the Shanghai Synchrotron Radiation Facility (SSRF). The surface morphologies of the films were characterized by SEM (JEOL JSM-7800F Prime). PL and TRPL spectra were measured at room temperature with controlled low humidity in air on an FLS1000 photoluminescence spectrometer (Edinburgh Instruments Ltd.) under a 450 nm excitation laser. The PL mapping was measured by inVia confocal Raman microscope. Current density-voltage curves of perovskite solar cells were measured by a Keithley 2401 source meter with a scan rate of 10 mV s^{-1} under simulated AM 1.5 G illumination (100 mW cm^{-2}; Enlitech Class AAA Solar Simulator). The EL spectra and EQE_{EL} was acquired by an Ocean Optics fiber spectrometer (QE 65 Pro, with an integration sphere) combined with a Keithley 2400 source meter. EQE was measured on an Enlitech QE-3011 system. The dark I-V for SCLC measurements were performed on devices with the structure of FTO/SnO_2/perovskite/PCBM/Ag using a Keithley 2401 source meter. The TPV (Zahner PP211 and Zahner Zennium) were generated by a microsecond pulse of a white light incident on solar cells under open circuit condition. The EIS measurements and Mott-Schottky plots were carried out using Zahner Zennium electrochemical workstation under dark condition. The operational stability was evaluated under MPP condition (100 mW cm^{-2} white LED lamp, Bamboo Technology) at around 50 °C in the N_2-filled glovebox without encapsulation.

Calculations

The charge carrier lifetime (τ_{ave}) was calculated from equation $\tau_{ave} = (A_1\tau_1^2 + A_2\tau_2^2)/(A_1\tau_1 + A_2\tau_2)$. Here, A_1 and A_2 denote the decay amplitudes. τ_1 and τ_2 denote the decay times.

The $\Delta V_{oc,non\text{-}rad}$ was calculated according to the formula: $\Delta V_{oc,non-rad} = kT\ln(EQE_{EL})/q$, where k, T, and q are Boltzmann constant, temperature, and elementary electric charge, respectively.

The relationship between $-dV/dJ$ and $(J_{sc}-J)^{-1}$ in Figure S14 was calculated from the relationship between V and J in dark for the prepared $FAPbI_3$ perovskite solar cells according to the following formula:

$$-\frac{dV}{dJ}=\frac{nkT}{q(Jsc-J)}+R_s$$

The relationship between ln (J_{sc}-J) and V+R$_s$$J$ in Figure S15 can be calculated from the relationship between V and J in dark for the prepared $FAPbI_3$ perovskite solar cells according to the following formula:

$$\ln{(Jsc-J)}=\frac{q}{nkT}(V+R_sJ)+lnJ_0$$

J_0 denotes saturated recombination current density.

Trap-state density (n_{trap}) was measured from trap-filled limit voltage (V_{TFL}), obtained from SCLC test of electron-only devices. The structure of electron-only device is FTO/c-TiO_2/SnO_2/perovskite/PCBM/Ag. The n_{trap} was calculated according to the following equation:

$$n_{trap}=2\varepsilon_0\varepsilon V_{TFL}/eL^2$$

Where e is the elementary charge, L is the thickness of the perovskite films, ε is the relative dielectric constant of perovskite film (46.9 for $FAPbI_3$)[1, 2] and ε_0 is the vacuum permittivity.

Supporting Figures

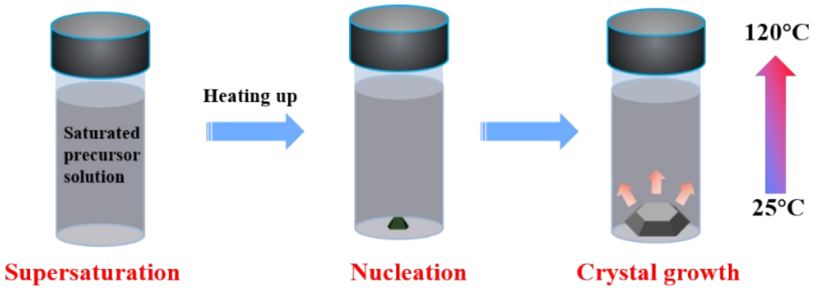

Fig. S1 Schematic process on the preparation of $FAPbI_3$ perovskite single crystal by inverse temperature crystallization.

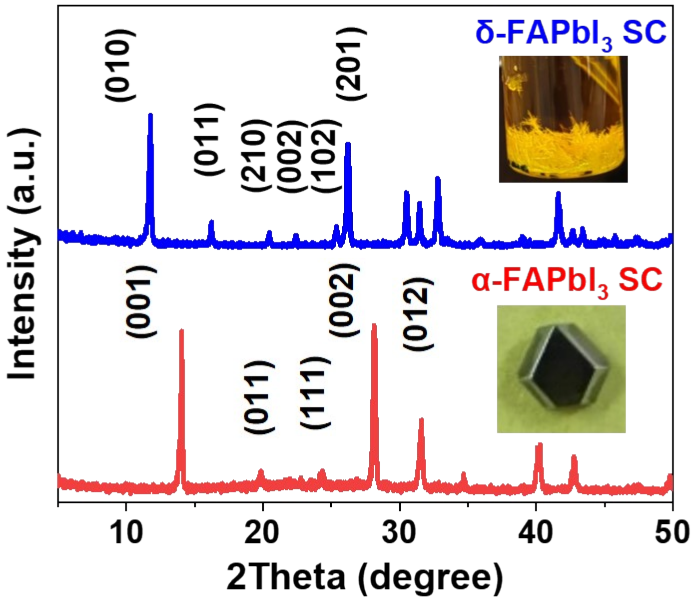

Fig. S2 XRD patterns and photographs (inset) of the synthesized black phase α-$FAPbI_3$ and yellow phase δ-$FAPbI_3$ perovskite single crystals.

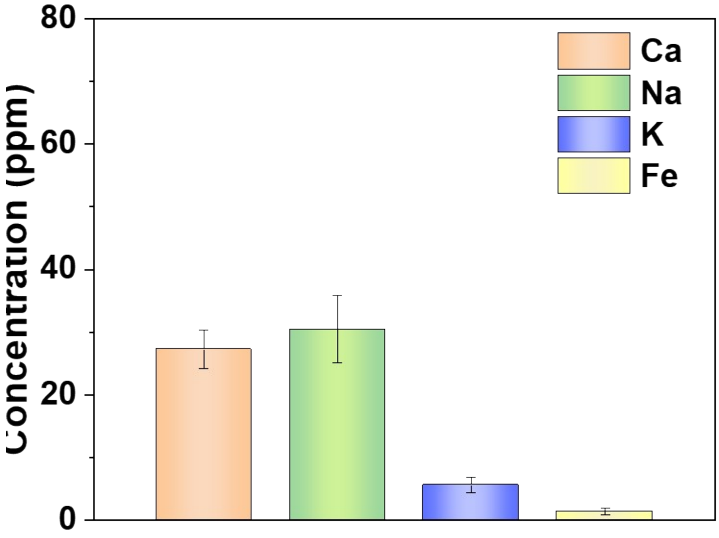

Fig. S3 Trace metal contents in α-$FAPbI_3$ single crystal prepared after 10 cycles of mother liquor.

Table S1. The materials cost (including cost on the raw materials and reaction solution) of the synthesized $FAPbI_3$ perovskite single crystals.

Raw material	Brand	Retail price US$ (quantity)	Experimental dosage	Experimental consumption	Yield

				US$	
FAAc	Bide Pharmatech	13.64 (500g)	329.5g	8.99	
HI (60%)	Adamas	898.3 (10kg)	736.1g	66.13	
PbI_2 (98%)	Macklin	21.13 (100g)	1313.85g	277.6	
GBL	Sinopharm Chemical Reagent Co., Ltd.	41.67 (500ml)	500ml	41.67	
δ-$FAPbI_3$ SCs					1582.50g (88.24 %)
α-$FAPbI_3$ SCs					1591.81g (87.72 %)
SUM				394.4	**0.2478 \$/g δ-$FAPbI_3$ SCs** **0.2492 \$/g α-$FAPbI_3$ SCs**

The data were obtained from the websites of Sinopharm Chemical Reagent Co., Ltd. (www.sinopharm.com), Macklin (www.macklin.cn), Bide Pharmatech (bidepharmatech.com) and Adamas (www.adamasbeta.com). The number of cycles for preparing yellow phase and black phase single crystals differs due to the influence of temperature on the lifespan of mother liquor. The yield calculation is based on 15 cycles of yellow-phase single crystal mother liquor and 10 cycles of black-phase single crystal mother liquor.

Table S2 The prices of commonly used commercial perovskite precursor materials.

Raw material	**Brand**	**Retail price US\$ (quantity)**	**\$/g**
PbI_2 (99.999%)	Aladdin	171(5g)	34.2
FAI (99.5%)	Macklin	47(1g)	47
SUM			**37.68\$/g $FAPbI_3$**

The data were obtained from the websites of Aladdin (www.aladdin-e.com) and Macklin (www.macklin.cn).

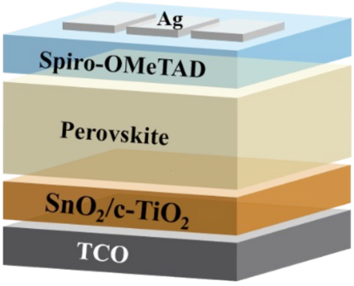

Fig. S4 Schematic device structure of the n-i-p perovskite solar cell.

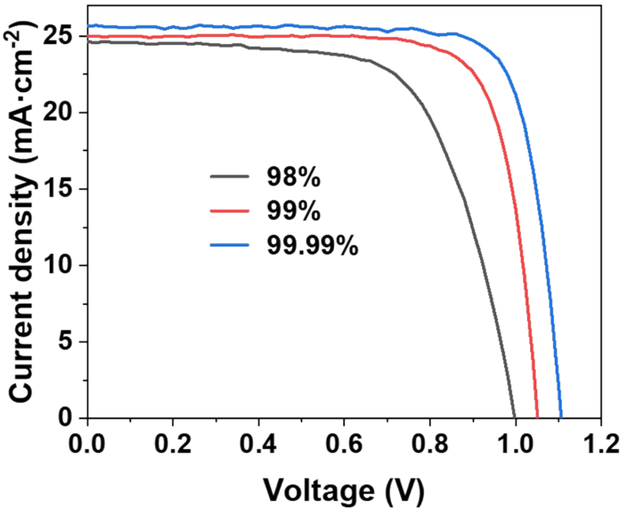

Fig. S5 Representative *J-V* curves of $FAPbI_3$ perovskite solar cells based on PbI_2+FAI precursor using lead iodides of different purity grades.

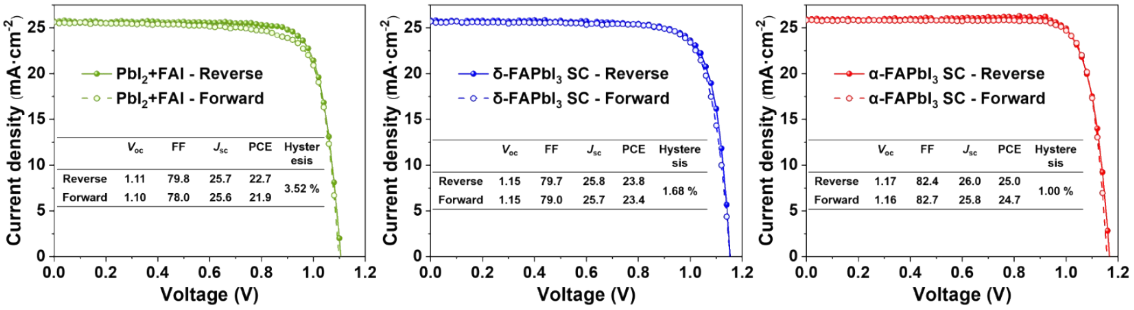

	V_{oc}	FF	J_{sc}	PCE	Hysteresis
Reverse	1.11	79.8	25.7	22.7	3.52 %
Forward	1.10	78.0	25.6	21.9	

	V_{oc}	FF	J_{sc}	PCE	Hysteresis
Reverse	1.15	79.7	25.8	23.8	1.68 %
Forward	1.15	79.0	25.7	23.4	

	V_{oc}	FF	J_{sc}	PCE	Hysteresis
Reverse	1.17	82.4	26.0	25.0	1.00 %
Forward	1.16	82.7	25.8	24.7	

Fig. S6 *J-V* curves of the best perovskite solar cells based on PbI_2+FAI, δ-$FAPbI_3$ and α-$FAPbI_3$ SCs under reverse scans and forward scans.

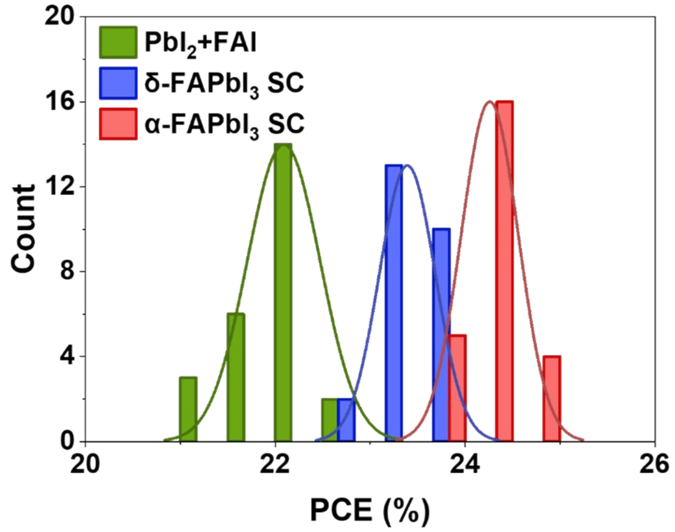

Fig. S7 PCE distribution of the devices based on PbI_2+FAI, δ-$FAPbI_3$ and α-$FAPbI_3$ SCs.

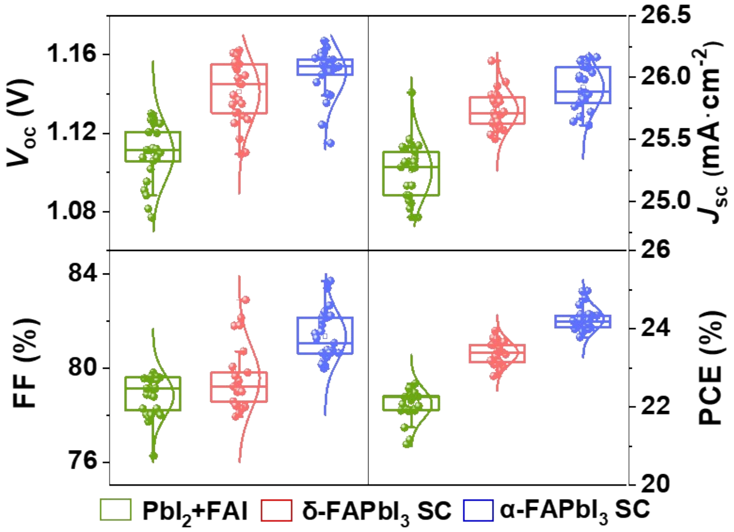

Fig. S8 Statistical PV parameters of the devices based on PbI_2+FAI, δ-$FAPbI_3$ and α-$FAPbI_3$ SCs.

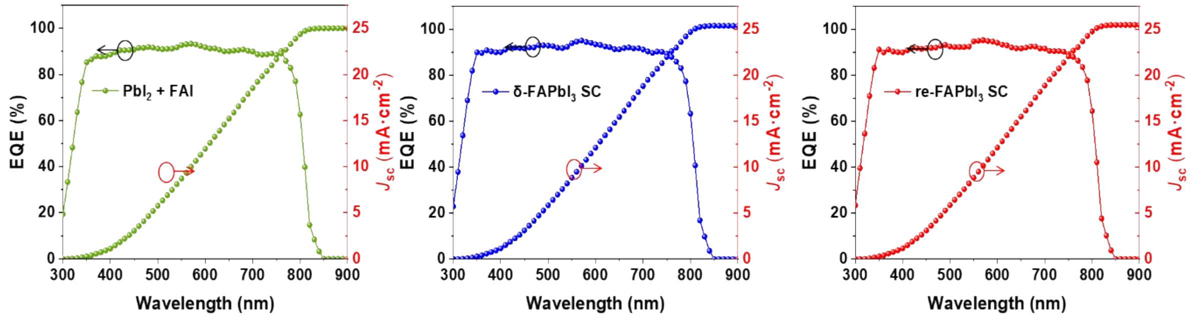

Fig. S9 EQE curves and integrated current densities of the perovskite solar cells based on PbI_2+FAI, δ-$FAPbI_3$ and α-$FAPbI_3$ SCs.

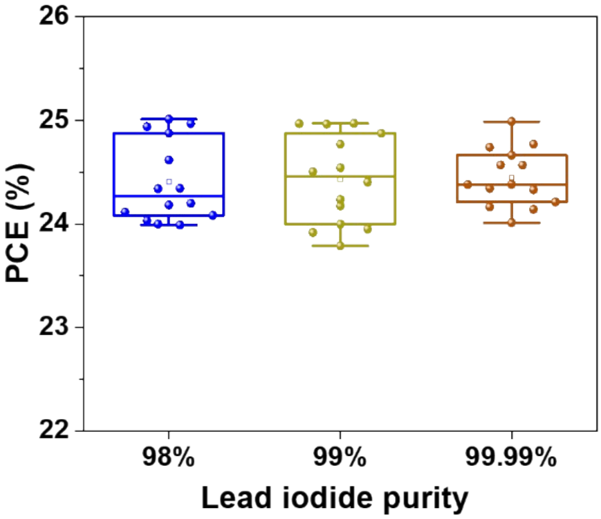

Fig. S10 Statistical PCE of perovskite solar cells based on $FAPbI_3$ single crystals that were prepared from lead iodides with different purity grades.

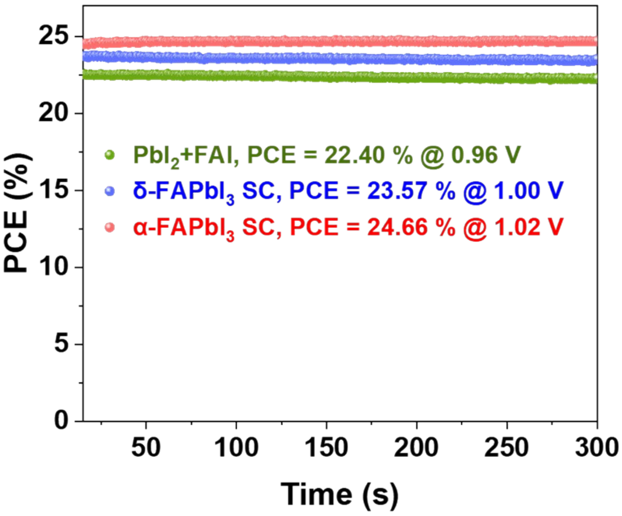

Fig. S11 Stabilized power output of the perovskite solar cells based on PbI_2+FAI, δ-$FAPbI_3$ and α-$FAPbI_3$ SCs.

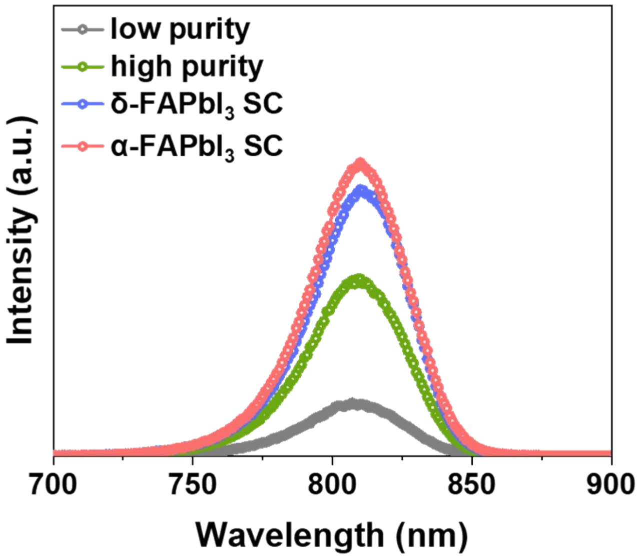

Fig. S12 PL spectra of the perovskite films based on low- and high-purity PbI_2+FAI, δ-$FAPbI_3$ and α-$FAPbI_3$ SCs

Table S3. Fitting parameters for TRPL spectra of the perovskite films prepared by PbI_2+FAI, δ-$FAPbI_3$ and α-$FAPbI_3$ single crystals and recrystallized α-$FAPbI_3$ single crystals.

	τ_{ave} (ns)	τ_1 (ns)	A_1	τ_2 (ns)	A_2
Low-purity PbI_2+FAI	40.89	1.61	0.44	42.27	0.48
High-purity PbI_2+FAI	73.58	2.97	0.52	77.54	0.36
δ-$FAPbI_3$ SC	88.89	15.92	0.22	93.05	0.65
α-$FAPbI_3$ SC	122.82	13.56	0.19	126.62	0.59

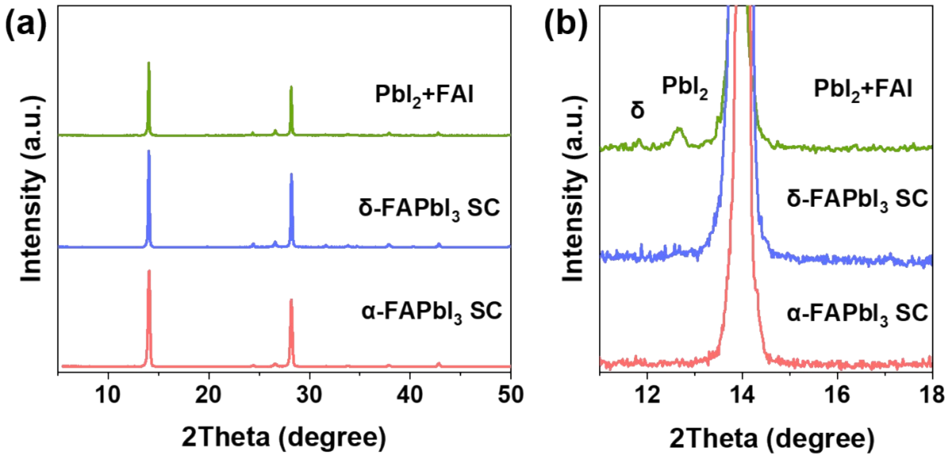

Fig. S13 (a) XRD patterns of perovskite films prepared by PbI_2+FAI, δ-$FAPbI_3$ and α-$FAPbI_3$ single crystal precursors. (b) Zoomed XRD patterns in the range of 11° to 18°.

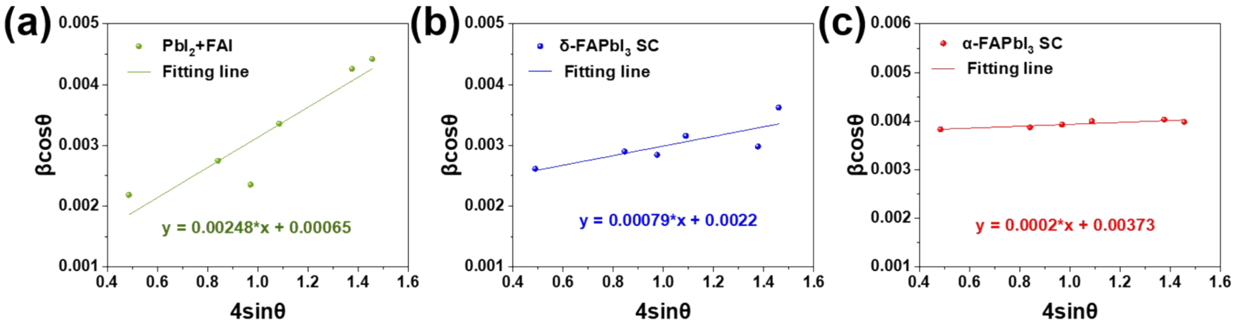

Fig. S14 W–H plots based on the XRD patterns of the perovskite films prepared by PbI_2+FAI (a), δ-$FAPbI_3$ (b) and α-$FAPbI_3$ (c) single crystal precursors.

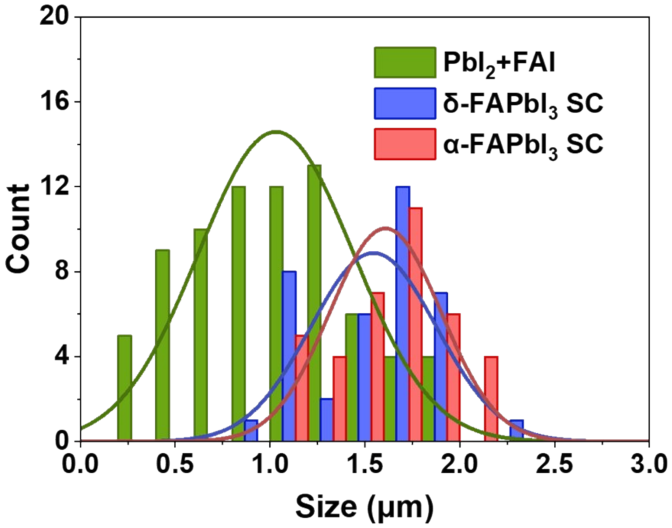

Fig. S15 Grain size distribution of the perovskite films prepared by PbI_2+FAI, δ-$FAPbI_3$ and α-$FAPbI_3$ single crystal precursors.

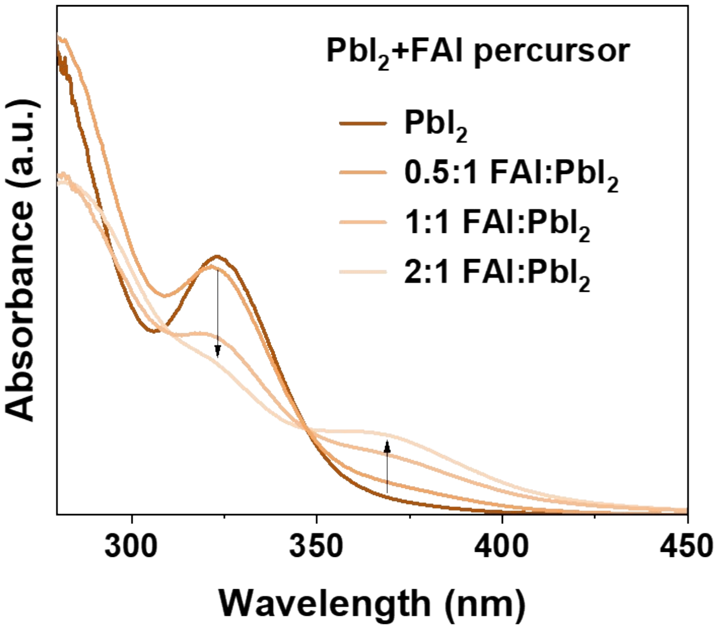

Fig. S16 UV-vis absorption spectra of diluted precursor solutions of PbI_2+FAI with different proportions.

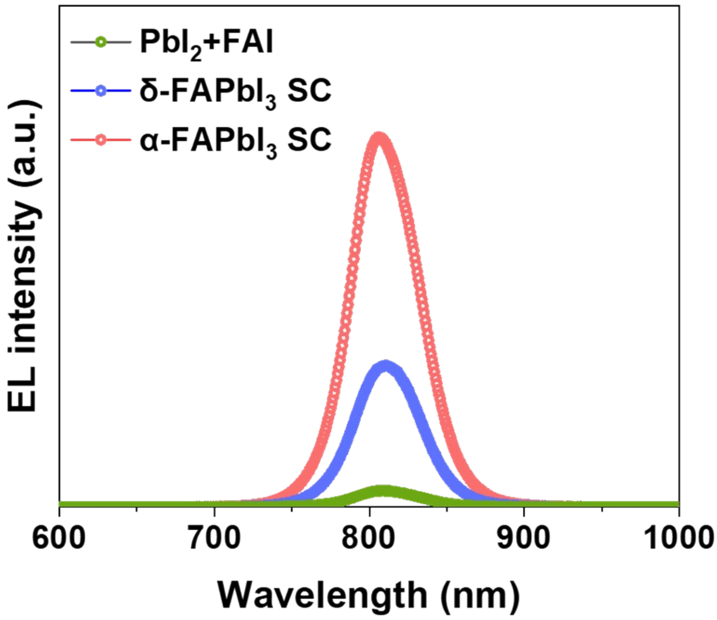

Fig. S17 EL spectra of the devices based on PbI_2+FAI, δ-$FAPbI_3$ and α-$FAPbI_3$ SCs.

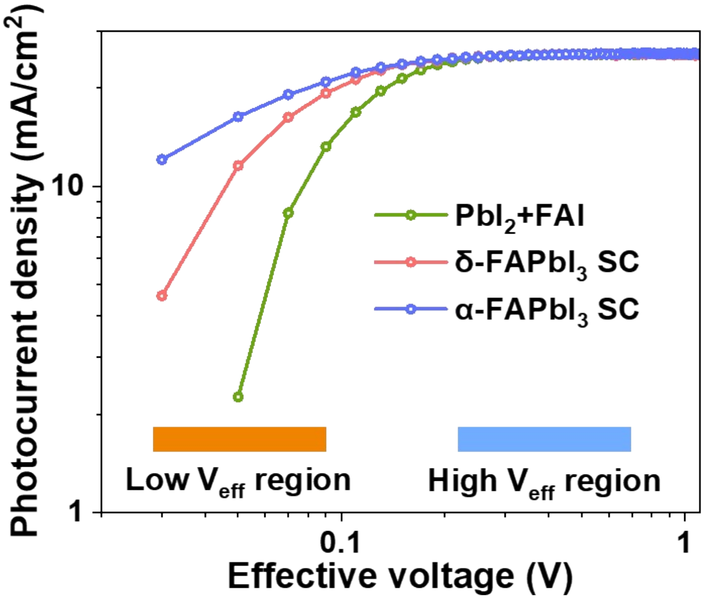

Fig. S18 Relationship between photocurrent density and effective voltage of the perovskite solar cells prepared by PbI_2+FAI, δ-$FAPbI_3$ and α-$FAPbI_3$ single crystal precursors.

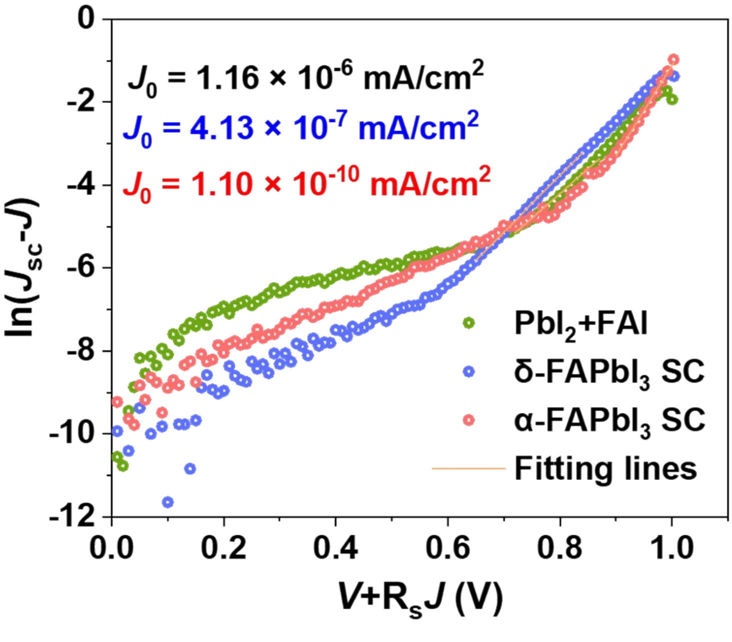

Fig. S19 Relationship between ln (J_{sc}-J) and V+R$_s$$J$ for the perovskite solar cells based on PbI_2+FAI, δ-$FAPbI_3$ and α-$FAPbI_3$ single crystal precursors.

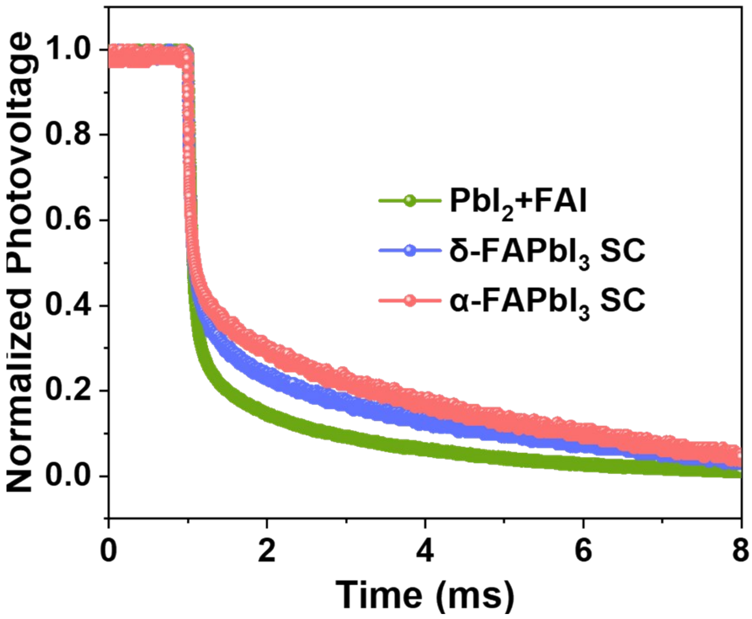

Fig. S20 TPV decay curves of the devices based on PbI_2+FAI, δ-$FAPbI_3$ and α-$FAPbI_3$ SCs.

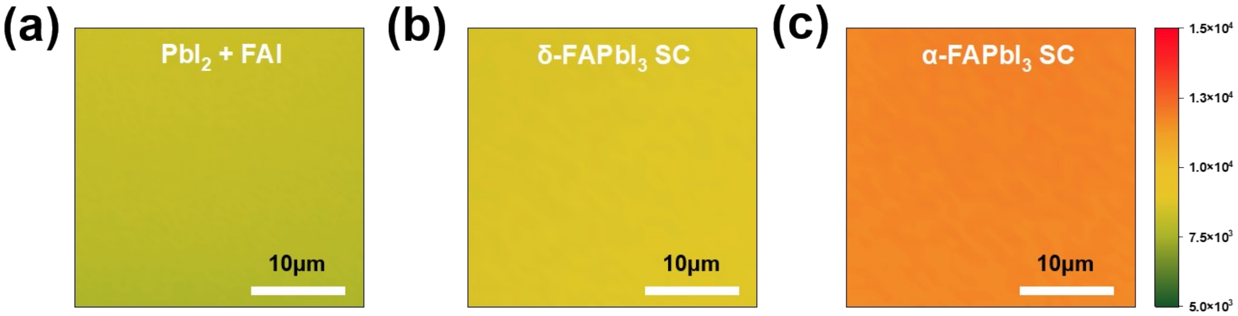

Fig. S21 (a-c) PL mapping intensity of the 2 cm × 2 cm sized $FAPbI_3$ perovskite films prepared by PbI_2+FAI, δ-$FAPbI_3$ and α-$FAPbI_3$ SCs (measurement region: 30 μm × 30 μm).

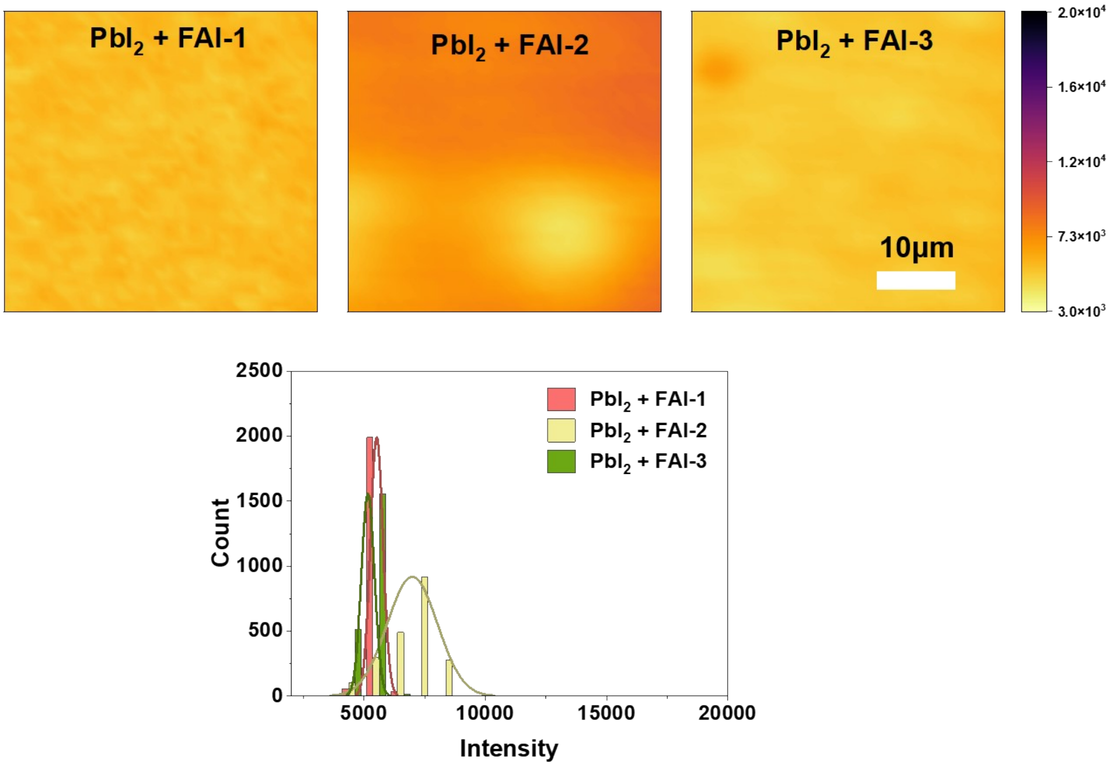

Fig. S22 PL mapping intensity and distribution of the 30 cm × 30 cm sized FAPbI$_3$ perovskite films at different locations prepared by PbI$_2$ + FAI precursor (measurement region: 40 μm × 40 μm).

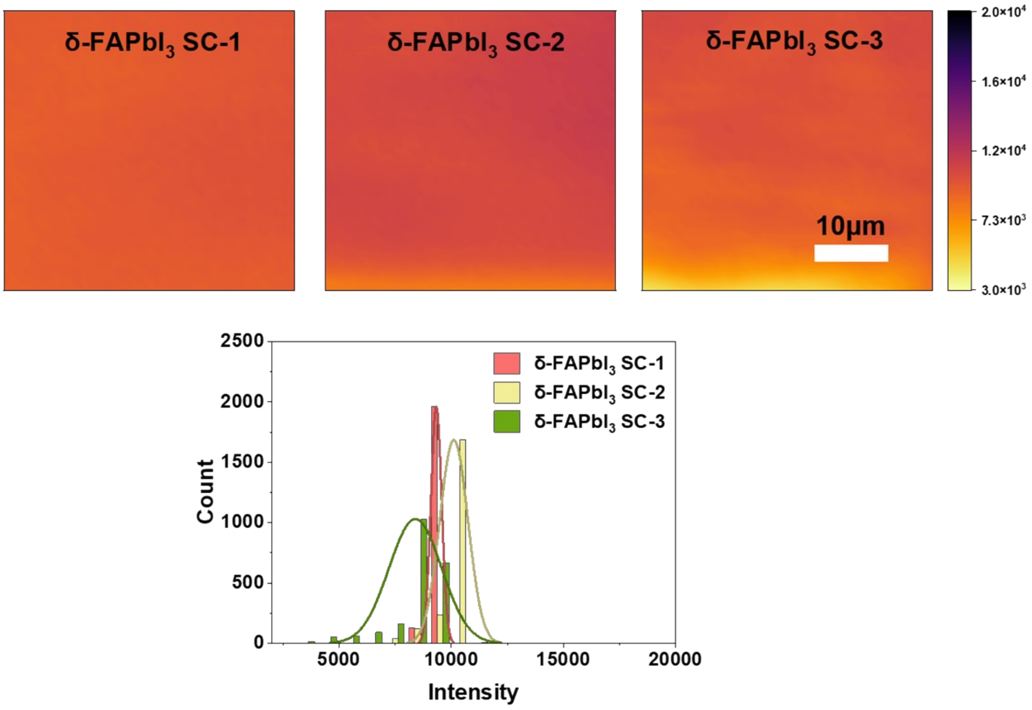

Fig. S23 PL mapping intensity and distribution of the 30 cm × 30 cm sized $FAPbI_3$ perovskite films at different locations prepared by δ-$FAPbI_3$ SC precursor (measurement region: 40 μm × 40 μm).

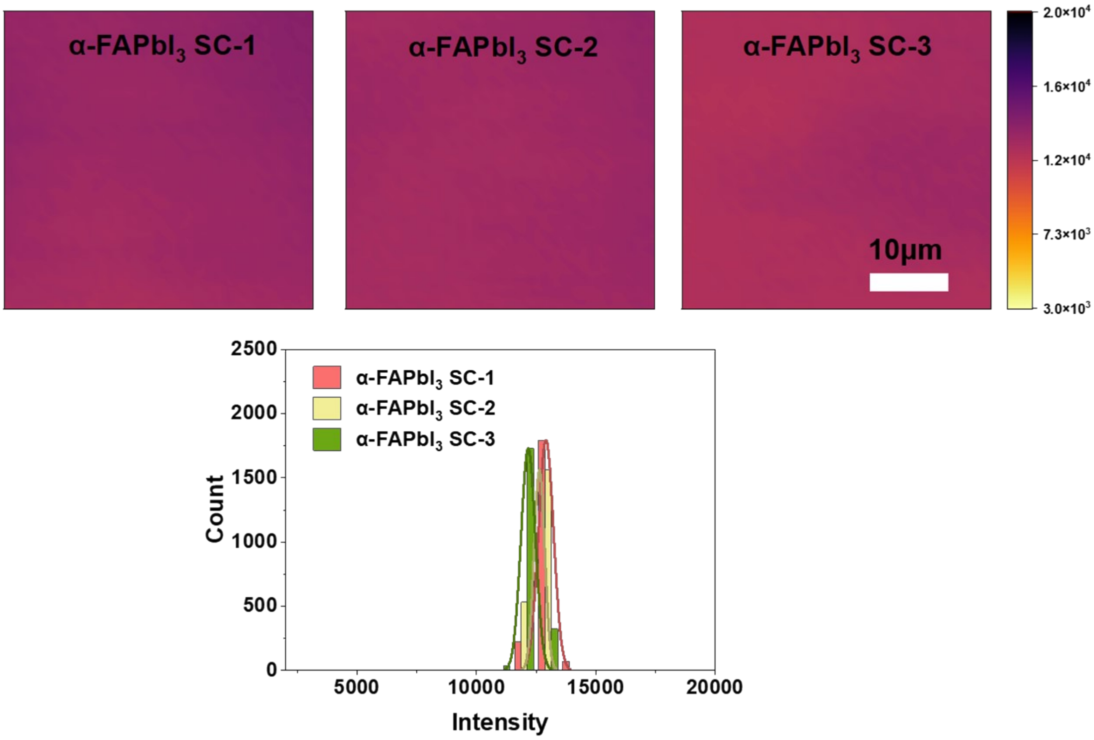

Fig. S24 PL mapping intensity and distribution of the 30 cm × 30 cm sized $FAPbI_3$ perovskite films at different locations prepared by α-$FAPbI_3$ SC precursor (measurement region: 40 μm × 40 μm).

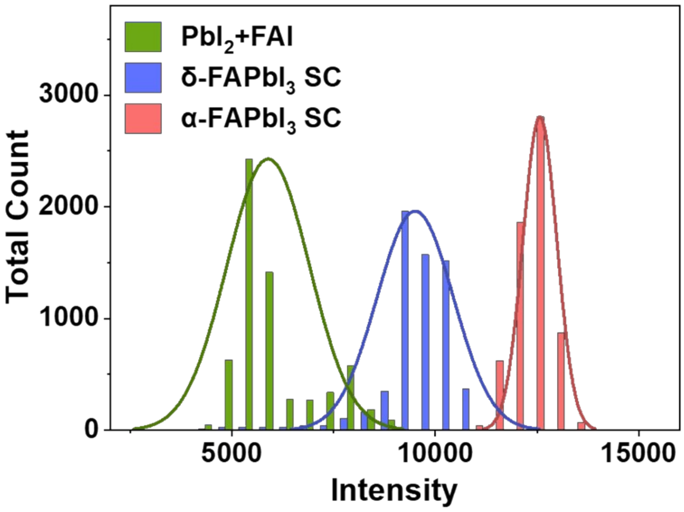

Fig. S25 Total PL mapping intensity distribution of the 30 cm x 30 cm sized $FAPbI_3$ perovskite films prepared prepared by PbI_2+FAI, δ-$FAPbI_3$ and α-$FAPbI_3$ single crystals (measurement region: 40 μm x 40 μm).

Table S4 Device parameters of the $FAPbI_3$ submodules prepared by PbI_2+FAI, δ-$FAPbI_3$ and α-$FAPbI_3$ single crystals.

	V_{oc} (V)	J_{sc} (mA/cm^2)	FF (%)	PCE (%)
PbI_2+FAI	56.4	0.452	69.0	17.6
δ-$FAPbI_3$ SC	57.6	0.451	75.9	19.7
α-$FAPbI_3$ SC	57.5	0.451	79.8	20.7

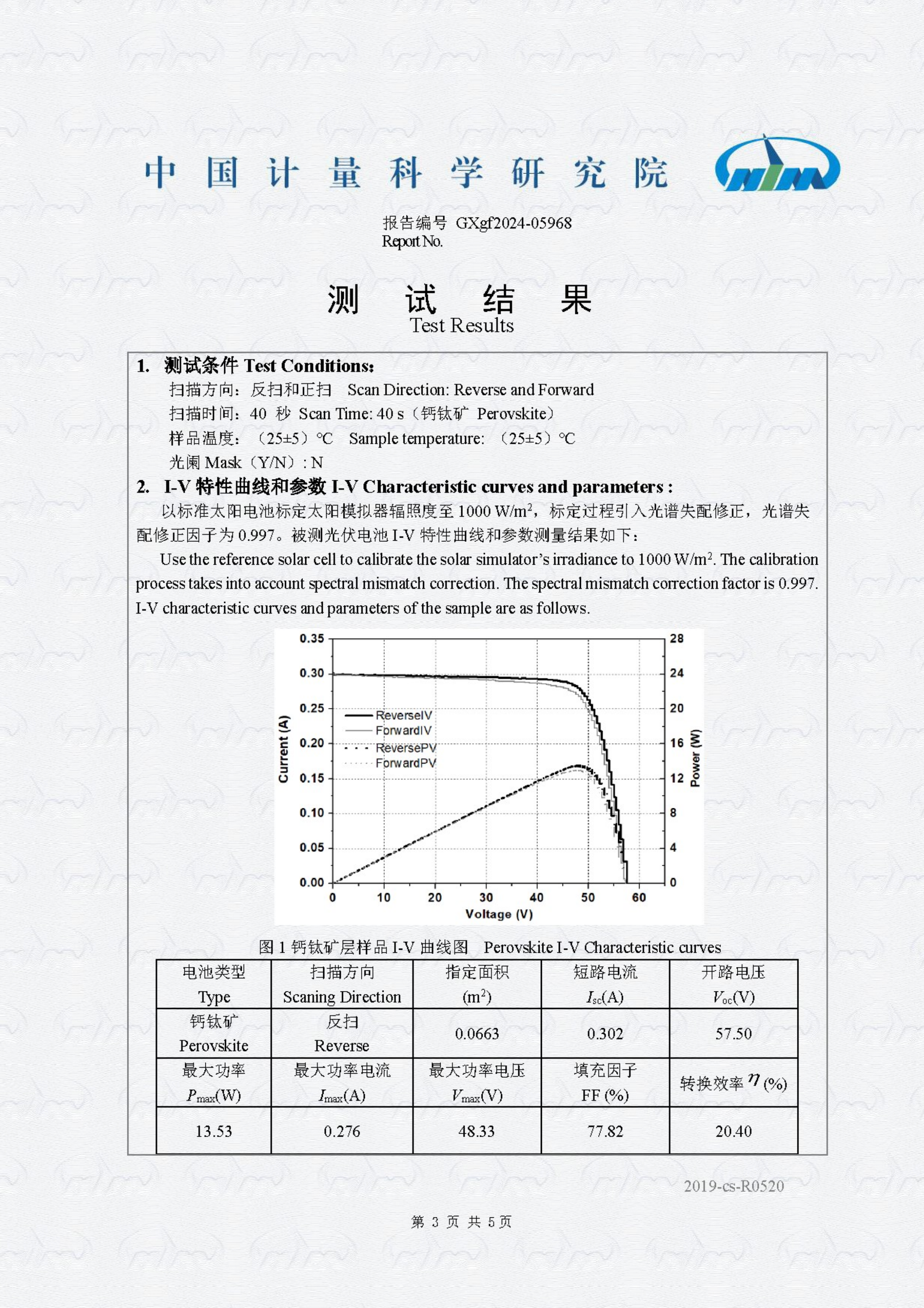

中 国 计 量 科 学 研 究 院

报告编号 GXgf2024-05968
Report No.

测 试 结 果
Test Results

1. 测试条件 Test Conditions:

扫描方向：反扫和正扫　Scan Direction: Reverse and Forward

扫描时间：40 秒 Scan Time: 40 s（钙钛矿 Perovskite）

样品温度：（25±5）℃　Sample temperature: （25±5）℃

光阑 Mask（Y/N）: N

2. I-V 特性曲线和参数 I-V Characteristic curves and parameters :

以标准太阳电池标定太阳模拟器辐照度至 1000 W/m^2，标定过程引入光谱失配修正，光谱失配修正因子为 0.997。被测光伏电池 I-V 特性曲线和参数测量结果如下：

Use the reference solar cell to calibrate the solar simulator’s irradiance to 1000 W/m^2. The calibration process takes into account spectral mismatch correction. The spectral mismatch correction factor is 0.997. I-V characteristic curves and parameters of the sample are as follows.

图 1 钙钛矿层样品 I-V 曲线图　Perovskite I-V Characteristic curves

电池类型 Type	扫描方向 Scaning Direction	指定面积 (m^2)	短路电流 I_{sc}(A)	开路电压 V_{oc}(V)
钙钛矿 Perovskite	反扫 Reverse	0.0663	0.302	57.50
最大功率 P_{max}(W)	最大功率电流 I_{max}(A)	最大功率电压 V_{max}(V)	填充因子 FF (%)	转换效率 η (%)
13.53	0.276	48.33	77.82	20.40

2019-cs-R0520

第 3 页 共 5 页

Fig. S26 Certified *I-V* curves of perovskite solar module with aperture area of 663 cm^2.

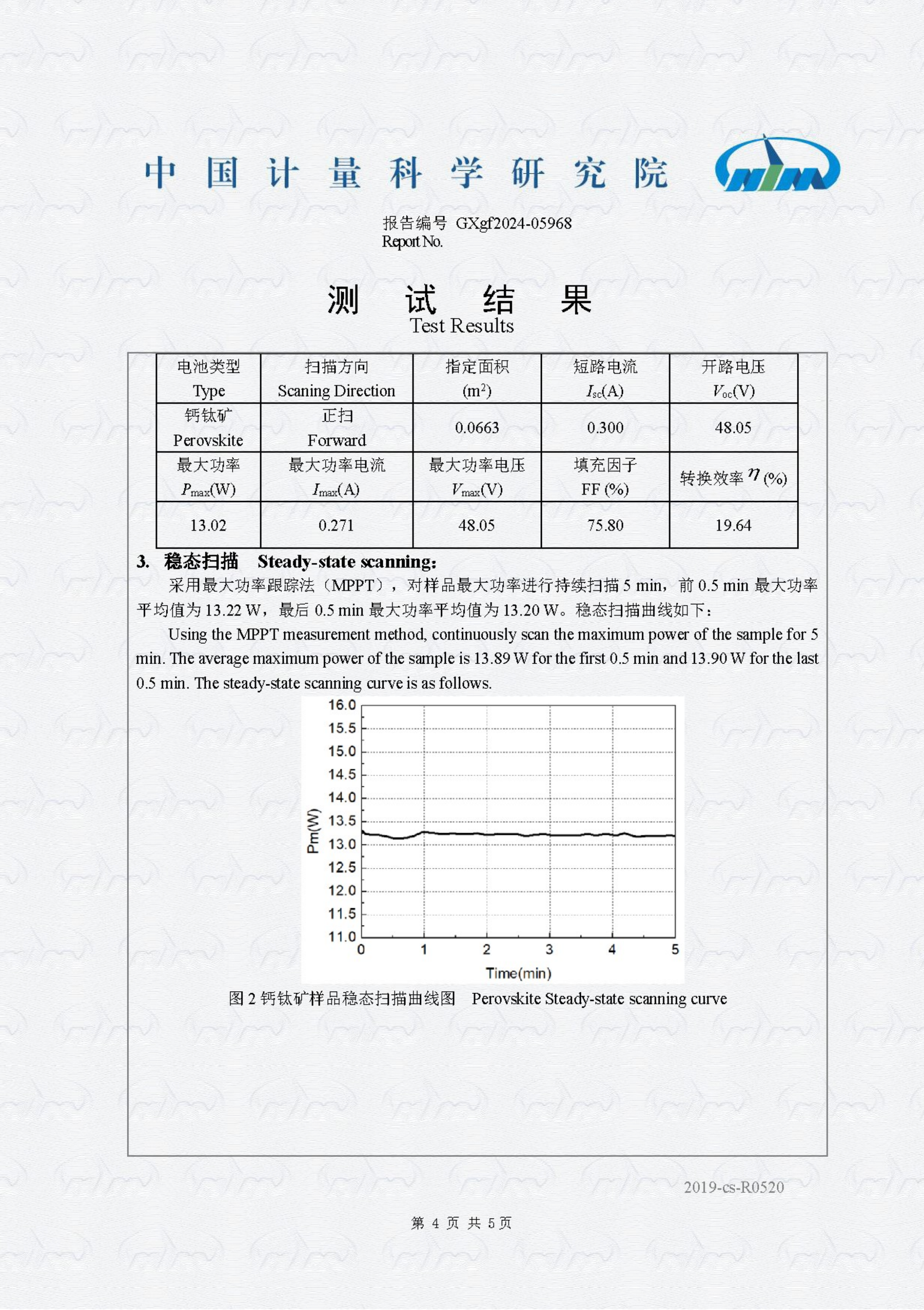

中 国 计 量 科 学 研 究 院

报告编号 GXgf2024-05968
Report No.

测 试 结 果
Test Results

电池类型 Type	扫描方向 Scaning Direction	指定面积 (m^2)	短路电流 I_{sc}(A)	开路电压 V_{oc}(V)
钙钛矿 Perovskite	正扫 Forward	0.0663	0.300	48.05
最大功率 P_{max}(W)	最大功率电流 I_{max}(A)	最大功率电压 V_{max}(V)	填充因子 FF (%)	转换效率 η (%)
13.02	0.271	48.05	75.80	19.64

3. 稳态扫描 Steady-state scanning:

采用最大功率跟踪法（MPPT），对样品最大功率进行持续扫描 5 min，前 0.5 min 最大功率平均值为 13.22 W，最后 0.5 min 最大功率平均值为 13.20 W。稳态扫描曲线如下：

Using the MPPT measurement method, continuously scan the maximum power of the sample for 5 min. The average maximum power of the sample is 13.89 W for the first 0.5 min and 13.90 W for the last 0.5 min. The steady-state scanning curve is as follows.

图 2 钙钛矿样品稳态扫描曲线图 Perovskite Steady-state scanning curve

2019-cs-R0520

第 4 页 共 5 页

Fig. S27 Certified maximum power point tracking of perovskite solar module with aperture area of 663 cm^2.

1. Q. Han, S.-H. Bae, P. Sun, Y.-T. Hsieh, Y. Yang, Y. S. Rim, H. Zhao, Q. Chen, W. Shi, G. Li and Y. Yang, *Adv. Mater.*, 2016, **28**, 2253-2258.
2. G. Chen, Y. Qiu, H. Gao, Y. Zhao, J. Feng, L. Jiang and Y. Wu, *Adv. Funct. Mater.*, 2020, **30**, 1908894.